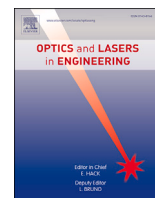




Contents lists available at ScienceDirect

Optics and Lasers in Engineering

journal homepage: www.elsevier.com/locate/optlaseng

Self-assembling of PDMS microlens arrays through pyro-EHD for real-time 3D microscopy

Nicolo Incardona^{a,b,*}, Sara Coppola^{a,*}, Veronica Vespini^a, Simonetta Grilli^a, Jaromir Behal^{a,c}, Lisa Miccio^a, Vittorio Bianco^a, Manuel Martinez-Corral^b, Pietro Ferraro^a

^a Institute of Applied Sciences and Intelligent Systems “E. Caianiello” (ISASI-CNR), via Campi Flegrei 34, 80078 Pozzuoli, Napoli, Italy

^b 3D Imaging and Display Laboratory, Department of Optics, Universitat de València, 46100 Burjassot, Spain

^c Department of Optics, Faculty of Science, Palacky University, 17. listopadu 12, 77146 Olomouc, Czechia

ARTICLE INFO

Keywords:

Self-assembling
Pyroelectric effect
Polymers
Microlenses
Lightfield
3D microscopy

ABSTRACT

The electrohydrodynamic effect has been exploited for the fabrication of polymeric microlenses through different approaches. Here we show that microlens arrays obtained with the pyro-EHD self-assembling process exhibit high fill-factor and good level of homogeneity, thus allowing to integrate them in a lightfield microscope. Digital holographic microscopy is used to characterize the fabricated microlens array. Afterwards, a Fourier lightfield microscope is built by placing this microlens array at the Fourier plane of the objective. We demonstrate for the first time that the self-assembled PDMS microlens array is suitable for 3D imaging of microscopic samples, computationally reconstructing the volume of a thick fluorescent sample.

1. Introduction

The recent advances in the fabrication of optical components have opened the way for a wide variety of applications. In this sense, microlens arrays (MLAs) are important elements for both optics and photonics fields. These micro-optical components have been integrated in several applications, such as 3D imaging and display [1,2], OLEDs [3], illumination [4], sensing [5,6] and solar cells [7]. Given the broadening of their applicability, there is an increasing effort in investigating innovative techniques for the fabrication of MLAs. In particular, several methods have been proposed to produce polymer MLAs, due to their affordability and good optical properties. Among them, we can mention micromolding [8], hot embossing [9], lithographic techniques [10], laser-based techniques [11,12], or ink-jet printing [13]. The choice of the fabrication method depends on factors such as the desired lens properties, the scale of the array, and the specific application requirements. Also, electrohydrodynamic (EHD) effect has been used for the fabrication of MLAs, through different approaches [14–16]. More recently, the pyroelectric effect has been employed for the first time to induce EHD instabilities, introducing a new phenomenon that we call pyro-EHD. In particular, the inkjet printing of microlenses has been obtained by pyro-EHD under different configurations [17,18]. The self-assembling process activated by pyro-EHD stands out for being highly straight-

forward and affordable. The fabrication of tunable liquid MLAs was demonstrated by using this technique [19]. Later, it was employed for the production of polymer MLA, with diameters ranging from 25 to 200 μm [20].

MLAs fabricated through pyro-EHD self-assembling exhibit a high degree of uniformity and can reach high fill factors. These characteristics make them perfect for their integration in lightfield (LF) systems. LF is an emerging 3D imaging technique, based on the insertion of an MLA in the optical path of a system with the aim of capturing the angular information of the rays emerging from a 3D object. The spatio-angular information recorded can be used to computationally retrieve the 3D volume of the objects captured or to project the 3D scene through an autostereoscopic display [1]. In the last two decades, this technique has been applied to 3D photography [21], display [22] and finally to microscopy [23]. As a proof of the growing interest in this technology, we can mention several companies that commercialize products based on LF technology, in the three applications cited [24–26]. In this work, we used the MLA to build a Fourier lightfield microscope (FLMic) [27]. In this system, the MLA is placed at the Fourier plane of the microscope objective, to capture an array of orthographic views of a 3D sample, from which it is possible to extract computationally its depth information. The reduced diameter of the microlenses used in the first kind of LF microscopes [23] (typically of the order of 100 μm) can be an im-

* Corresponding authors at: 3D Imaging and Display Laboratory, Department of Optics, Universitat de València, 46100 Burjassot, Spain.
E-mail addresses: nicolo.incardona@uv.es (N. Incardona), sara.coppola@isasi.cnr.it (S. Coppola).

<https://doi.org/10.1016/j.optlaseng.2024.108239>

Received 16 October 2023; Received in revised form 28 March 2024; Accepted 7 April 2024

Available online 17 April 2024

0143-8166/© 2024 The Author(s). Published by Elsevier Ltd. This is an open access article under the CC BY-NC license (<http://creativecommons.org/licenses/by-nc/4.0/>).

pairing factor for the optical performance of FLMic systems. In fact, placing the MLA at the Fourier plane of the objective, its effective aperture is reduced. Therefore, the use of microlenses of small diameter would compromise excessively the resolution of the system.

Based on the requirements set by the optical system, we fabricated a custom-made MLA through the pyro-EHD self-assembling process. We patterned a Lithium Niobate (LN) crystal with a square array of reversed polarization domains, having a period of 0.5 mm, in order to obtain an array of microlenses of 0.5 mm diameter. So far, these are the biggest microlenses fabricated through the self-assembling approach compared with previous fabrication procedures [28]. Polydimethylsiloxane (PDMS) was the polymer used for the fabrication of the MLA. PDMS is a widely used material in microfluidics and micro-optics due to its optical transparency, biocompatibility, and ease of fabrication. These qualities make it attractive for various applications in micro-optics and integrated optical systems. The resulting MLA was characterized by means of digital holography (DH). Here we demonstrate for the first time that we are able to fabricate self-assembled MLA via pyro-EHD with microlenses diameters up to 0.5 mm and fill-factor close to 1. So far, the maximum diameter achieved for microlenses manufactured by this method was 0.2 mm. By integrating such novel MLA into a modified FLMic set-up, we proved that this optical system could be exploited to image a thick fluorescent sample, a category which several biological specimens (e.g. thick tissue slides, organoids, model organisms) belong to. We visualize the reconstructed volume of the sample, thus demonstrating the feasibility of the self-fabricated MLA to image microscopic 3D objects.

2. Material and methods

2.1. Fourier lightfield microscope

For a better understanding of the motivations behind the election of the geometry of the MLA to fabricate, a brief description of the optical system in which it will be integrated is necessary. LF microscopy is a 3D microscopy technique based on the simultaneous capture, by means of an MLA, of spatial and angular information of the rays emerging from the sample. From the spatio-angular map acquired, the 3D information of the specimen can be calculated using different algorithms based on ray optics [29], wave optics [30,31] or even artificial intelligence [32]. The ability to capture depth information in a single shot makes LF technique suitable for the observation of 3D fast dynamic samples. For this reason, LF microscopy has been applied especially to biological living samples [33–35].

One of the main issues of LF systems is the intrinsic trade-off between lateral and angular resolution. In fact, the capability of recording angular information comes at the price of losing lateral resolution, which is a fundamental parameter in microscopy. For this reason, several set-ups have been presented since the first proposal of LF microscope, in which the MLA was placed at the image plane of a conventional microscope [23]. Among them, FLMic [27] improves lateral resolution, provides lateral shift invariance and avoids the inhomogeneity of the reconstruction resolution typical of the aforementioned first implementation. In FLMic, the MLA is placed at the Fourier plane of the microscope objective. In Fig. 1, the classic implementation of an FLMic is shown, in which a 4f relay system (lenses $RL1$ - $RL2$) is used to conjugate the aperture stop of the objective with the MLA. The sensor (CMOS camera), placed at the image plane of the microlenses, captures an array of orthographic views of the sample, each one from a slightly different angle. The aperture stop of the microscope objective is the element that determines its light gathering capability. The field stop, instead, is usually an iris diaphragm that is placed at the intermediate image plane to avoid overlapping between the orthographic (or angular) views.

The lateral resolution limit, ρ , of an optical microscope depends on the numerical aperture (NA) of its objective, through:

$$\rho = \frac{\lambda}{2NA} \quad (1)$$

where λ is the wavelength of the light scattered or emitted by the sample. The NA of an objective is usually provided by the manufacturers and it is related to the aperture stop diameter, Φ_{AS} , by:

$$NA = \frac{\Phi_{AS}}{2f_{Ob}} \quad (2)$$

being f_{Ob} the focal length of the objective. In an FLMic, the effective aperture of the objective is determined by the diameter of the microlenses of the MLA. For the sake of clarity, let us represent the FLMic omitting the relay lenses, as shown in Fig. 2. To consider the contribution of the relay system, it is sufficient to scale the diameter and focal length of the microlenses: $\Phi_{ML,as} = \frac{f_1}{f_2}\Phi_{ML}$ is the equivalent diameter of the microlenses at the aperture stop plane. Therefore, the effective numerical aperture of the microscope objective in an FLMic is:

$$NA_{eff} = \frac{\Phi_{ML,as}}{2f_{Ob}} \quad (3)$$

Hence, to minimize the lateral resolution loss, the diameter of the microlenses should not be excessively small. Ideally, three microlenses should fit into the diameter of the aperture stop to have acceptable angular information without sacrificing excessively the lateral resolution. Moreover, also the field of view (FOV) of each angular view directly depends on the size of the microlenses:

$$FOV = \frac{f_2}{f_1} \frac{f_{Ob}}{f_{ML}} \Phi_{ML} \quad (4)$$

as well as the number of pixels, L , that compose each angular view:

$$L = \frac{\Phi_{ML}}{\delta} \quad (5)$$

where δ is the pixel size in the sensor. We set a diameter $\Phi_{ML} = 0.5$ mm for the fabrication of the MLA, to have a productive combination for all the above parameters and following [36]. It is noteworthy that the fabrication of microlenses of this size represents a challenge for the pyro-EHD self-assembling technique.

2.2. MLA fabrication

Pyro-EHD self-assembling technique is based on the use of a functionalized ferroelectric crystal. A thin film of liquid or polymer is deposited onto the functionalized crystal. Heating the substrate causes uncompensated charges distributions, that provoke hydrodynamic instability in the liquid or polymer. This leads to the self-assembling of the thin film into an array of microstructures. The reader can refer to the first publications of the group [19,28] for a deeper understanding of the phenomenon. If the crystal is coated with a polymer that could be cured by temperature or dissolved in the proper solvent, the application of high temperatures induces the simultaneous curing of the material, leading to the formation of a stable MLA.

In this work, the crystal used as the substrate to build the polymer MLA is a z-cut, optically polished and 500 μm thick LN crystal from Crystal Technology. LN is a well-known ferroelectric material, whose polarization can be reversed through electric field poling [37]: an external voltage exceeding the intrinsic coercive field of the material (21 kV/mm approximately) was applied to reverse the polarization. The final polarization pattern was achieved by means of a resist grating obtained through photolithography. The pattern used consists of hexagonal domains having minimal diameter 0.25 mm, disposed in a square array with period 0.5 mm in both x and y directions. Fig. 3 shows the schematic view of the periodically poled LN (PPLN) crystal.

PDMS (Polydimethylsiloxane, Sylgard 184, Dow Corning Corp, Midland; $\eta = 3900$ cP, $\epsilon_p = 2.65$ from datasheet) base elastomer was mixed with the curing agent with a ratio of 10:1. Then, it was spin coated onto the PPLN crystal. The crystal with the polymer film was

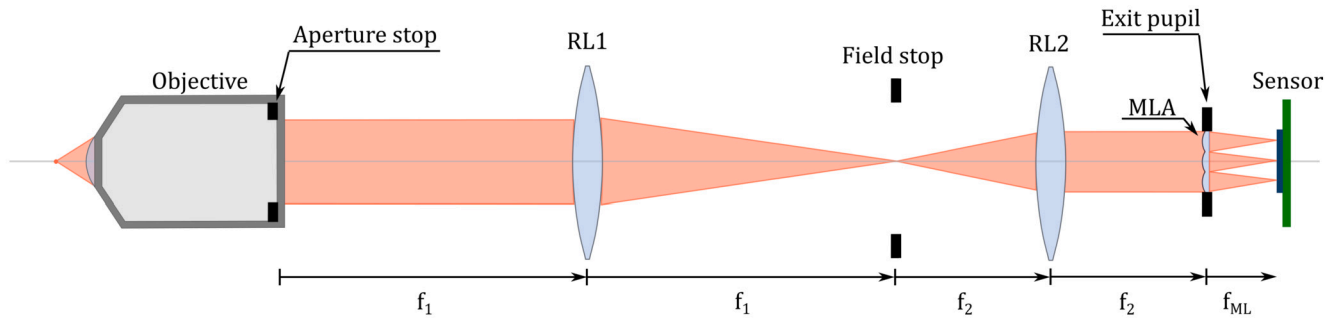


Fig. 1. The optical scheme of the FLMic. The lenses *RL1* and *RL2* compose a double telecentric relay, that conjugates the aperture stop of the objective with the MLA: the exit pupil is the image of the aperture stop of the microscope objective. The sensor is a commercial CMOS camera.

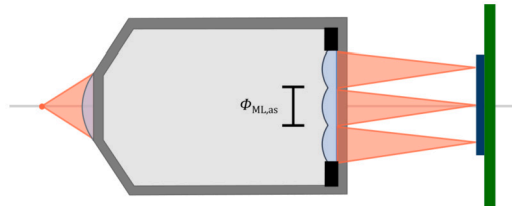


Fig. 2. Optical scheme of the FLMic when the relay system is omitted. The aperture of the objective is limited by the scaled diameter of the microlenses.

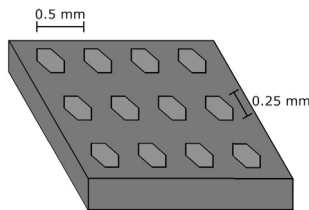


Fig. 3. Schematic view of the PPLN, with a square array of hexagonal reversed domains. The period is 0.5 mm and the internal diameter of the hexagonal domains is 0.25 mm.

placed onto a glass microscope slide and put on a hot plate at 110 °C for 10 minutes. The thermal stimulus activates the pyro-EHD effect that provokes the self-assembling of the polymer into an MLA, following the pattern of the functionalized LN crystal. At the same time, the high temperature induces the curing of the polymer, producing a stable MLA.

The self-assembling of PDMS MLAs guided by the pyro-EHD effect has been already demonstrated: in [20], several PPLN crystals were used to fabricate multiscale PDMS MLAs with microlenses of up to 0.2 mm diameter. Here, the authors showed that the final shape of the microlenses can be adjusted varying the parameters of the fabrication process. In particular, the focal length strongly depends on the thickness of the polymer layer (i.e., on the spinning speed). Microlenses of higher focal lengths are obtained for thicker PDMS layers (that is, for lower spinning speeds). Other parameters influencing the final shape of the microlenses include the choice of the crystal side onto which the polymer is spin coated (Z+ or Z- side) and the applied thermal stimulus. This behaviour was deeply characterized in the aforementioned work. In our case, we needed microlenses bigger than those obtained in [20], not to compromise the lateral resolution of the final optical system in which they are integrated. Being the first time that such a high period was used to pattern the LN crystal, the fabrication of high-quality MLAs was not trivial. In fact, the uniformity in size and shape is essential for consistent optical performance across the MLA. To overcome these challenges and achieve high-quality MLAs with large periods, several experiments were conducted for the fabrication of the MLA, varying the thickness of the PDMS film (that is, varying the spinning speed) and the crystal side. We observed that for spinning speeds lower than 2000 rpm, the microstructures obtained applying the thermal stimulus

were not stable. When the PPLN with the polymer film was put onto the hot plate, we could observe the formation of the MLA, but this MLA collapsed after few seconds. This behaviour was observed for spinning speeds 1000 rpm, 1500 rpm and 1800 rpm, for PDMS deposited onto both Z+ and Z- crystal sides. On the other hand, for spinning speeds greater than 3000 rpm, the microlenses of the array appeared to be separated, leading to diameter $\Phi_{ML} < 0.5 \text{ mm}$, that would result in a loss of lateral resolution. The best result was achieved for spinning speed equal to 2000 rpm and Z+ side of the crystal. Therefore, after its characterization, the MLA obtained with these experimental parameters was used to build the FLMic.

3. Results

3.1. MLA characterization

To characterize quantitatively the fabricated MLA, we built a digital holographic microscope. DH is a powerful tool for the quantitative analysis of materials [38,39]. The optical scheme of the set-up is shown in Fig. 4. The camera is a UI-2280SE-M from IDS Imaging, equipped with a CMOS sensor having 2448×2048 pixels of $3.45 \mu\text{m}$ side. The total magnification of the system is $M = 8.66$, which provides a FOV of $975 \times 816 \mu\text{m}^2$. With this FOV, two microlenses can be captured simultaneously. In the digital holographic microscope, the light proceeding from a laser source is first collimated and then split into two arms. The bottom arm in Fig. 4 is the signal arm: the collimated beam is used to illuminate the sample (in this case, the fabricated MLA), which is observed through a microscope objective. The signal is made to interfere with the reference beam (proceeding from the reference arm on top) and the hologram is recorded by the camera. By demodulating the digital hologram captured by the camera, the amplitude and phase of the light transmitted by the MLA under observation are reconstructed computationally. From this information, the 3D shape of the sample can be computed.

Fig. 5 shows the recorded digital hologram and the results of the reconstruction process. In particular, the phase map retrieved numerically from the digital hologram is shown in Fig. 5(b). The unwrapped phase map [40] is shown in Fig. 5(c) and it is represented three-dimensionally in Fig. 5(d). As expected, the microlenses show a continuous profile (so, $\Phi_{ML} = 0.5 \text{ mm}$). The unwrapped phase of another microlens of the array is shown in Fig. 5(g). From a first qualitative analysis of these results, it seems that the microlenses are not perfectly symmetric. The shape of the fabricated microlenses depends, among other factors, on the geometry of the array of the reversed polarization domains. The real geometry of the PPLN slightly differs from an ideal square array of 0.5 mm period. These errors in the layout can provoke a non-perfect spherical shape of the self-assembled microlenses. To demonstrate their sphericity, we extracted the cross-sectional distribution of the phase along the vertical and diagonal meridians of one microlens, which in Fig. 5(c) are indicated with a green and a purple dotted line, respectively. The corresponding phase profiles are shown in Fig. 5(e) and (f)

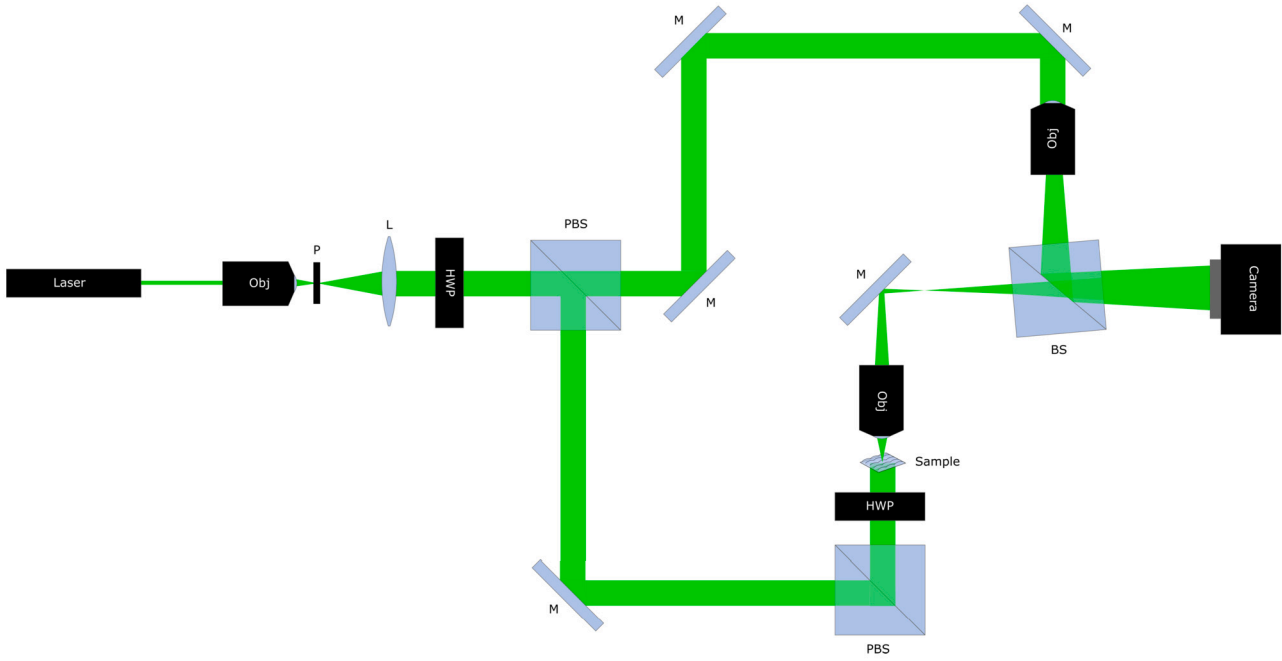


Fig. 4. The optical scheme of the digital holographic microscope. In the scheme, *Obj* stands for microscope objective, *P* is a pinhole, *L* is a converging lens, *HWP* is a halfwave plate, *M* is a mirror, *BS* is a beam splitter and *PBS* is a polarizing beam splitter.

and both compared with the same fitted sphere. The mean value of the two R-square parameters is 0.97, which demonstrates a good spherical shape of the microlens. The focal length of one lens can be calculated by fitting its unwrapped phase map with a second order polynomial and following this equation:

$$\Phi(x, y) = \frac{2\pi}{\lambda} \frac{(x^2 + y^2)}{2f}. \quad (6)$$

We estimated the focal length of multiple microlenses of the array and we calculated its mean value and its standard deviation: $f_{ML} = 4.1 \pm 0.2 \text{ mm}$. The relative error is 4.9%, which indicates a good consistency of the fabrication. The mean numerical aperture is $NA_{ML} = 0.061$, similar to the NA of commercially available MLAs.

3.2. Optical set-up

Once the MLA was fabricated and characterized, the components of the FLMic could be chosen, so to optimize the performances of the system. To do so, we first set two of the elements, namely the objective and the camera. The objective used was an infinity-corrected $10 \times / 0.25$ Nikon objective, having focal length $f_{Ob} = 20 \text{ mm}$ and diameter of the aperture stop $\Phi_{AS} = 10 \text{ mm}$. The camera is a UI-1460SE-C-HQ from IDS Imaging, equipped with a CMOS sensor having 2048×1536 pixels of size $\delta = 3.2 \mu\text{m}$. Unfortunately, this camera is not board-level. This represents an issue, as the physical distance between the first surface of the camera and the sensor is longer than the focal length of the MLA. This makes impossible to place the sensor at the image plane of the microlenses to capture the focused orthographic views of the sample. For this reason, we had to modify the traditional set-up of an FLMic that we showed in Fig. 1, including an additional 4f relay system to conjugate the image plane of the MLA with the camera sensor. Besides solving this issue, this second relay permits to improve the performances of the system if its magnification is set greater than 1. In fact, this increases the total magnification of the system:

$$M_t = \frac{f_1}{f_{Ob}} \frac{f_{ML}}{f_2} \frac{f_4}{f_3} \quad (7)$$

being f_3 and f_4 the focal lengths of the first and the second lens of this second relay, respectively. This leads to the improvement of the resolu-

tion limit given by Nyquist criterion, which in FLMic is not negligible as it usually happens in conventional microscopes:

$$\rho_{Nyq} = \frac{2\delta}{M_t}. \quad (8)$$

Moreover, the number of pixels along the diameter of each angular view is increased:

$$L = \frac{f_4}{f_3} \frac{\Phi_{ML}}{\delta}. \quad (9)$$

The lenses of both 4f relays must be chosen based on two necessary conditions for the operation of the system. The first one is that the minimum number of microlenses that fit entirely into the diameter of the exit pupil must be greater than 3 [27]:

$$N = \frac{\Phi_{AS}}{\Phi_{ML,as}} = \frac{f_2}{f_1} \frac{\Phi_{AS}}{\Phi_{ML}} > 3. \quad (10)$$

The second condition is that the diameter of the image of the pupil must be shorter than the sensor side:

$$\frac{f_4}{f_3} \left(\frac{f_2}{f_1} \Phi_{AS} \right) < 2048 \times 3.2 \mu\text{m}. \quad (11)$$

These requirements set the conditions for the magnification of the relays. After some experiment with diverse relay magnifications, we set $\frac{f_2}{f_1} = 0.25$ and $\frac{f_4}{f_3} = 2$. In addition, since Nikon objectives are designed to work in combination with a tube lens of 200 mm focal length, we chose the lenses of the relay systems as follows: $f_1 = 200 \text{ mm}$, $f_2 = 50 \text{ mm}$, $f_3 = 100 \text{ mm}$, $f_4 = 200 \text{ mm}$.

Despite permitting the conjugation of the MLA back focal plane with the sensor and increasing the total magnification of the system, the insertion of the second relay system provokes a different issue. The modified FLMic is no longer orthographic, that is, the lateral magnification is not constant, but it depends on the axial position of the object. In Fig. 6, we show graphically this problem by a simple ray-tracing for two identical objects placed at two different axial positions. This issue is provoked by the fact that the *RL2-MLA* compound is not in afocal configuration.

A straightforward solution is to shift the MLA from the exit pupil plane and place it in afocal configuration with the lens *RL2*. This will

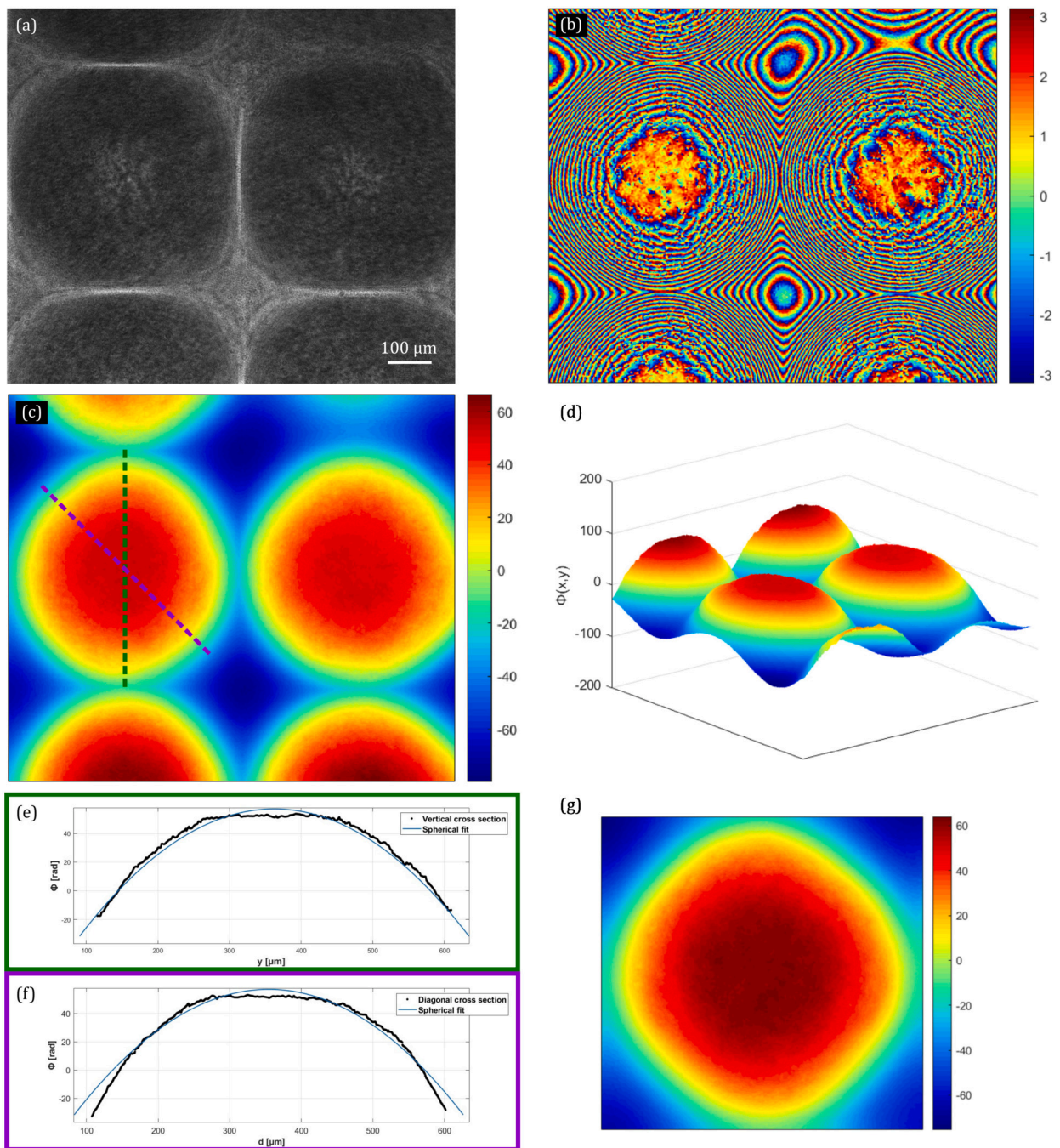


Fig. 5. Quantitative characterization of the fabricated MLA through digital holography. (a) The digital hologram recorded. (b) The wrapped phase map, modulo 2π . (c) The unwrapped phase map. (d) The 3D representation of the unwrapped phase map. (e)-(f) The phase profile along the vertical meridian and the diagonal meridian indicated in (c), respectively, and its comparison with an ideal spherical profile. (g) The unwrapped phase map of another microlens of the array.

cause vignetting effects in the microlenses that are at the edge of the exit pupil, given that the MLA is now placed onto a defocused image of the aperture stop. However, with the components chosen, we have that the number of microlenses that fit into the diameter of the exit pupil is $N = 5$. Therefore, even discarding the angular views that suffer vignetting effects, it is possible to reconstruct the volume of the 3D sample. Obviously, this is not an optimal solution, but it is useful to demonstrate the functioning of the FLMic with the fabricated MLA. To solve this problem, it will be sufficient to use a board-level camera, with no physical barrier between the sensor and the MLA.

The final set-up is shown in Fig. 7. The system was aligned using a He-Ne laser (black tube behind the optical set-up). To illuminate the sample, a compact laser module ($\lambda = 532 \text{ nm}$) was employed and a high-

pass filter was placed after the objective to filter out the light from the illumination module.

3.3. Sample imaging and reconstruction

To demonstrate the imaging capabilities of the optical system built with the self-assembled MLA, we used a simple object consisting of cotton fibers of a common lens cleaning paper, stained with the fluorescent ink of a highlighter. The fibers intersect forming a 3D structure that can be observed through the FLMic. The image captured by the sensor is shown in Fig. 8(a), with the central orthographic view zoomed for a better visualization. As can be seen, the number of complete views in a row is slightly greater than 4: due to the vignetting effect, we do not reach

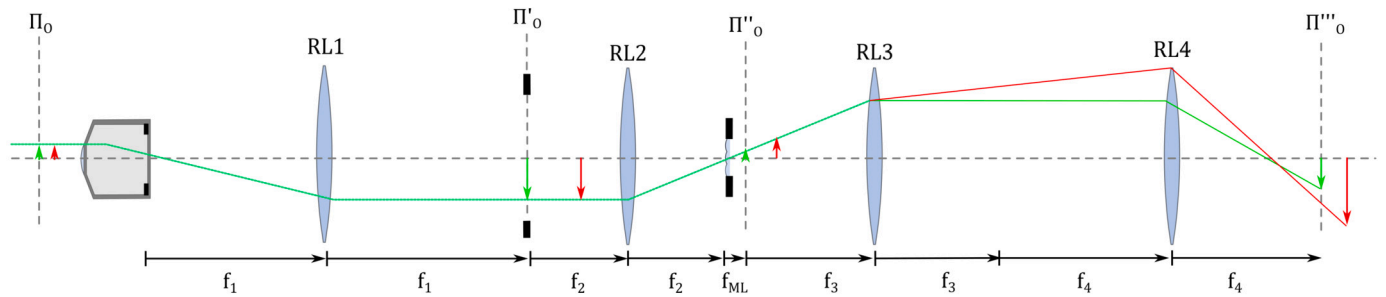


Fig. 6. The optical scheme of the FLMic when the second relay RL3-RL4 is inserted without modifying the position of other lenses. The ray tracing is shown for two identical objects at different axial positions: the green arrow is at the object plane of the microscope objective, while the red arrow is closer to the objective. At the final image plane (Π'''_0), the size of the images of the objects is different.

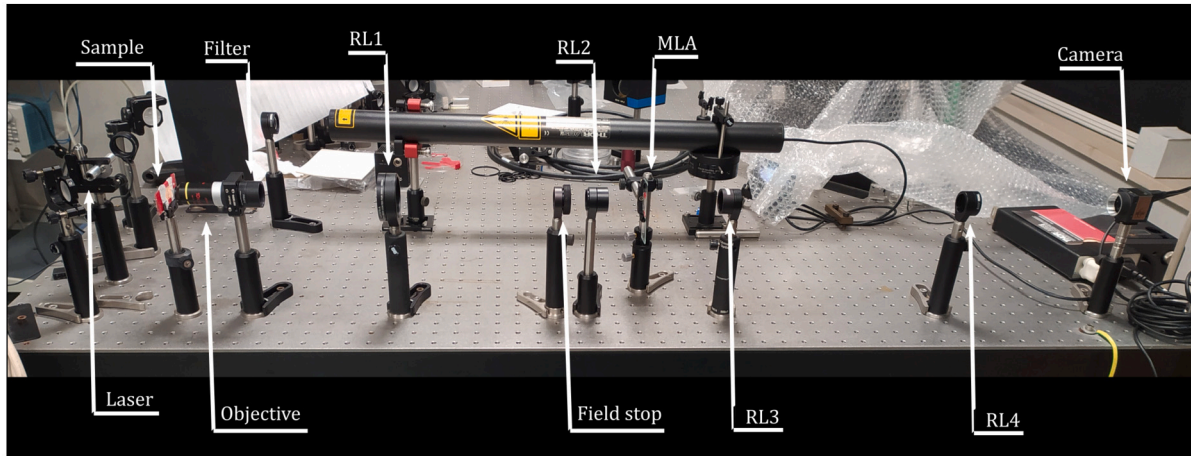


Fig. 7. The set-up of the modified FLMic with all its components indicated.

the theoretical value of $N = 5$. Despite the presence of background in the perspective views, the sample is imaged with a good contrast, which allows us to reconstruct its 3D volume.

For the 3D reconstruction, we applied a ray-optics based reconstruction algorithm designed for sparse samples [29]. Prior to the application of the algorithm, we performed the background subtraction by a simple tophat filtering. This enhances the contrast and the optical sectioning capability of the mentioned reconstruction algorithm. The total depth of reconstruction is ~ 1 mm, with an axial step between each plane that depends on the optical system [27]:

$$\Delta = \left(\frac{f_2}{f_1} \frac{f_{Ob}}{f_{ML}} \right)^2 \frac{f_{ML}}{\Phi_{ML}} \frac{f_3}{f_4} \delta = 20.5 \text{ } \mu\text{m}. \quad (12)$$

In Fig. 8(b), the sample reconstructed at different depths is shown. In particular, we show the reconstruction depths at which the different fibers come into focus. In the Supplementary Material, Movie S1 shows the entire focal stack and Movie S2 shows the 3D shape of the sample. From this representation, the 3D structure can be visualized, with the different fibers overlapping at different heights.

4. Conclusions

In this paper, we have demonstrated the viability of the pyro-EHD self-assembling technique for fabricating polymer MLA to integrate in a 3D microscopy system. The optical system sets the requirements for the fabrication of the MLA. Specifically, FLMic requires microlenses with bigger diameter with respect to the MLA fabricated previously with the pyro-EHD self-assembling method. We produced an MLA with microlenses of 0.5 mm diameter, demonstrating the straightforward scalability of the pyro-EHD low cost self-assembling process in respect to the previous state of the art of the fabrication method. The MLA

was observed under a digital holographic microscope, to characterize quantitatively the 3D shape of the microstructures. We confirmed that the fabricated microlenses have 0.5 mm and we estimated their focal length. After the characterization, the MLA was integrated in an FLMic, modifying the traditional set-up to deal with the issue related to the MLA-sensor distance. After choosing all the components and building the set-up, the FLMic was used to image a fluorescent 3D sample. Finally, the volume of the sample was computationally extracted. By imaging and reconstructing the object, we proved that the self-assembled polymer MLA is suitable for observing a microscopic 3D sample. Therefore, these microlenses represent a flexible and cost-effective alternative to the traditional glass MLA. The future work will be focused on the optimization of the MLA for improving the performances of the FLMic in terms of resolution and image quality.

CRediT authorship contribution statement

Nicolo Incardona: Conceptualization, Investigation, Methodology, Software, Visualization, Writing – original draft. **Sara Coppola:** Investigation, Methodology. **Veronica Vespini:** Conceptualization, Methodology. **Simonetta Grilli:** Conceptualization. **Jaromir Behal:** Resources, Software. **Lisa Miccio:** Resources. **Vittorio Bianco:** Resources. **Manuel Martinez-Corral:** Conceptualization, Supervision. **Pietro Ferraro:** Conceptualization, Supervision.

Declaration of competing interest

The authors declare that they have no known competing financial interests or personal relationships that could have appeared to influence the work reported in this paper.

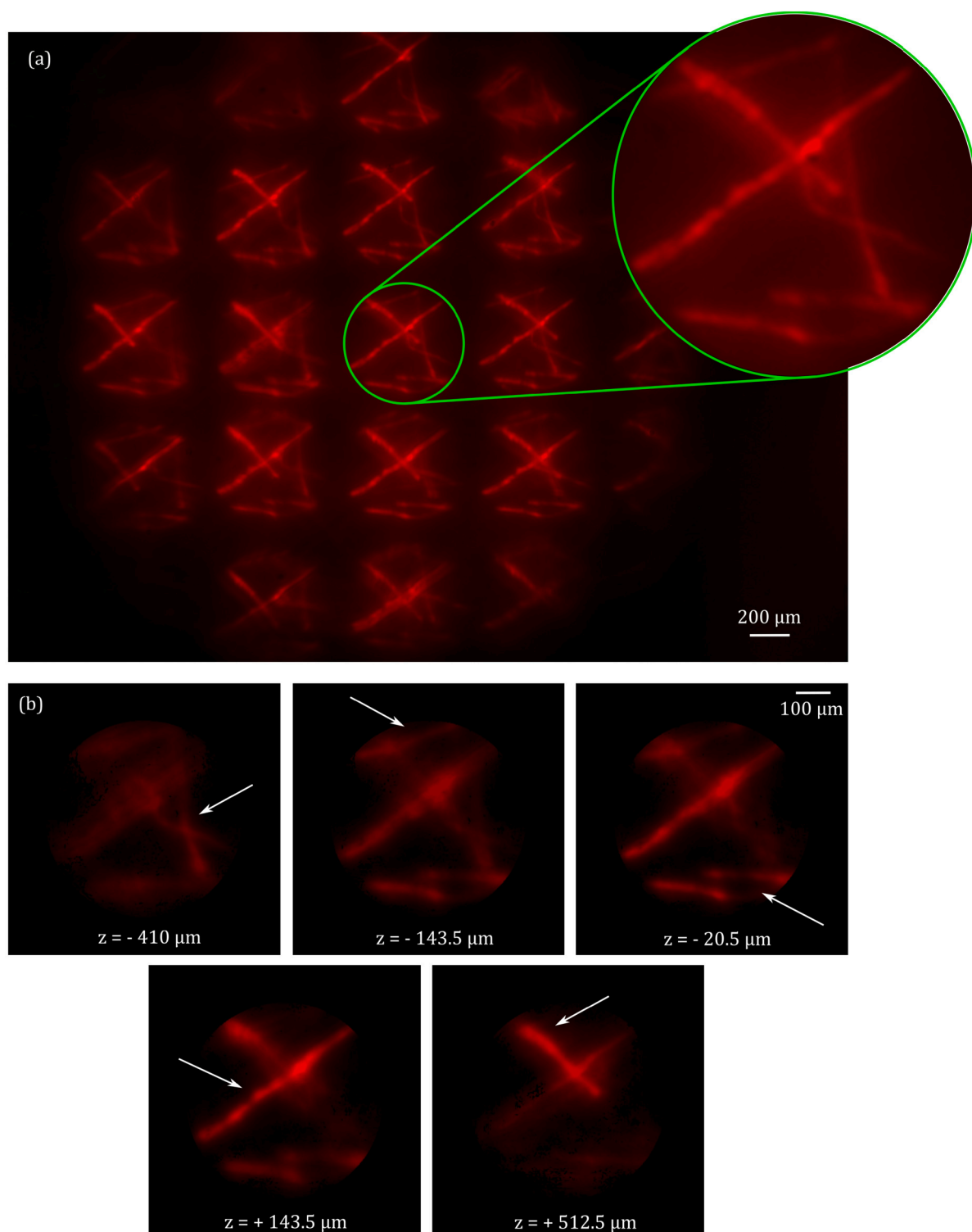


Fig. 8. (a) The image of the fluorescent cotton fibers captured with the FLMic. The central perspective view is zoomed for a better visualization. (b) The sample reconstructed at different depths. We have included only the planes at which some portion of the 3D object come into focus. The depth is given relative to the object plane: z has negative values for planes that are beyond the object plane (further from the objective) and positive values for planes closer to the objective than the object plane. The white arrows point at the fibers focused at each reconstruction plane. See Movie S1 of Supplementary Material for the complete focal stack.

Data availability

The data that has been used is confidential.

Acknowledgements

This work was supported by internal CNR funding [grant BIOLENS]; Ministerio de Ciencia, Innovación y Universidades, Spain, and European Regional Development Fund [grant PID2022-137747OB-I00]; Generalitat Valenciana, Spain [grant CIPROM/2022/30]. Nicolò Incardona is recipient of the Grant “Margarita Salas” (ref. MS21-141) for the requalification of the Spanish university system proposed by Ministerio de Universidades (Spain) and funded by the European Union, NextGenerationEU.

Appendix A. Supplementary material

Supplementary material related to this article can be found online at <https://doi.org/10.1016/j.optlaseng.2024.108239>.

References

- Martínez-Corral M, Javidi B. Fundamentals of 3d imaging and displays: a tutorial on integral imaging, light-field, and plenoptic systems. *Adv Opt Photonics* 2018;10:512–66.
- Javidi B, Carnicer A, Arai J, Fujii T, Hua H, Liao H, et al. Roadmap on 3d integral imaging: sensing, processing, and display. *Opt Express* 2020;28:32266–93.
- Qu Y, Kim J, Coburn C, Forrest SR. Efficient, nonintrusive outcoupling in organic light emitting devices using embedded microlens arrays. *ACS Photonics* 2018;5:2453–8.
- Coumans FA, van der Pol E, Terstappen LW. Flat-top illumination profile in an epifluorescence microscope by dual microlens arrays. *Cytometry, Part A* 2012;81:324–31.
- Intermite G, McCarthy A, Warburton RE, Ren X, Villa F, Lussana R, et al. Fill-factor improvement of si cmos single-photon avalanche diode detector arrays by integration of diffractive microlens arrays. *Opt Express* 2015;23:33777–91.
- Zhou W, Raasch TW, Allen YY. Design, fabrication, and testing of a shack-hartmann sensor with an automatic registration feature. *Appl Opt* 2016;55:7892–9.
- Fang C, Zheng J, Zhang Y, Li Y, Liu S, Wang W, et al. Antireflective paraboloidal microlens film for boosting power conversion efficiency of solar cells. *ACS Appl Mater Interfaces* 2018;10:21950–6.
- Zhu Jh, Shi Jx, Wang Y, He Ps. Spherical micro-lens array of pmma produced by micro-molding. *Chin J Chem Phys* 2006;19:443.
- Moore S, Gomez J, Lek D, You BH, Kim N, Song IH. Experimental study of polymer microlens fabrication using partial-filling hot embossing technique. *Microelectron Eng* 2016;162:57–62.
- Chang SI, Yoon JB. Shape-controlled, high fill-factor microlens arrays fabricated by a 3d diffuser lithography and plastic replication method. *Opt Express* 2004;12:6366–71.
- Ou Y, Yang Q, Chen F, Deng Z, Du G, Wang J, et al. Direct fabrication of microlens arrays on pmma with laser-induced structural modification. *IEEE Photonics Technol Lett* 2015;27:2253–6.
- Surdo S, Carzino R, Diaspro A, Duocastella M. Single-shot laser additive manufacturing of high fill-factor microlens arrays. *Adv Opt Mater* 2018;6:1701190.
- Luo Y, Wang L, Ding Y, Wei H, Hao X, Wang D, et al. Direct fabrication of microlens arrays with high numerical aperture by ink-jetting on nanotextured surface. *Appl Surf Sci* 2013;279:36–40.
- Li X, Ding Y, Shao J, Tian H, Liu H. Fabrication of microlens arrays with well-controlled curvature by liquid trapping and electrohydrodynamic deformation in microholes. *Adv Mater* 2012;24:OP165–9.
- Li H, Duan Y, Shao Z, Zhang W, Li H, Yang W, et al. Morphology-programmable self-aligned microlens array for light extraction via electrohydrodynamic printing. *Org Electron* 2020;87:105969.
- Im B, Prasetyo FD, Yudistira HT, Khalil SM, Cho DH, Byun D. Drop-on-demand electrohydrodynamic jet printing of microlens array on flexible substrates. *ACS Appl Polym Mater* 2023;5:2264–71.
- Ferraro P, Coppola S, Grilli S, Paturzo M, Vespini V. Dispensing nano-pico droplets and liquid patterning by pyroelectrodynamics. *Nat Nanotechnol* 2010;5:429–35.
- Vespini V, Coppola S, Todino M, Paturzo M, Bianco V, Grilli S, et al. Forward electrohydrodynamic inkjet printing of optical microlenses on microfluidic devices. *Lab Chip* 2016;16:326–33.
- Miccio L, Finizio A, Grilli S, Vespini V, Paturzo M, De Nicola S, et al. Tunable liquid microlens arrays in electrode-less configuration and their accurate characterization by interference microscopy. *Opt Express* 2009;17:2487–99.
- Vespini V, Gennari O, Coppola S, Nasti G, Mecozzi L, Pagliarulo V, et al. Electrohydrodynamic assembly of multiscale pdms microlens arrays. *IEEE J Sel Top Quantum Electron* 2014;21:399–406.
- Ng R, Levoy M, Brédif M, Duval G, Horowitz M, Hanrahan P. Light field photography with a hand-held plenoptic camera. Ph.D. thesis. Stanford University; 2005.
- Martínez-Cuenca R, Saavedra G, Martínez-Corral M, Javidi B. Progress in 3-d multi-perspective display by integral imaging. *Proc IEEE* 2009;97:1067–77.
- Levoy M, Ng R, Adams A, Footer M, Horowitz M. Light field microscopy. In: *Accm siggraph 2006 papers*; 2006. p. 924–34.
- Looking glass factory. <https://lookingglassfactory.com/>. [Accessed 13 December 2021].
- Raytrix. <https://raytrix.de/>. [Accessed 23 June 2022].
- Digital optical imaging technologies. <https://www.doitplenoptic.com/>. [Accessed 14 July 2023].
- Scrofanì G, Sola-Pikabea J, Llavador A, Sanchez-Ortiga E, Barreiro J, Saavedra G, et al. Fimic: design for ultimate 3d-integral microscopy of in-vivo biological samples. *Biomed Opt Express* 2018;9:335–46.
- Grilli S, Miccio L, Vespini V, Finizio A, De Nicola S, Ferraro P. Liquid micro-lens array activated by selective electrowetting on lithium niobate substrates. *Opt Express* 2008;16:8084–93.
- Sanchez-Ortiga E, Scrofanì G, Saavedra G, Martínez-Corral M. Optical sectioning microscopy through single-shot lightfield protocol. *IEEE Access* 2020;8:14944–52.
- Incardona N, Tolosa A, Saavedra G, Martínez-Corral M, Sanchez-Ortiga E. Fast and robust wave optics-based reconstruction protocol for Fourier lightfield microscopy. *Opt Lasers Eng* 2023;161:107336.
- Zhang Y, Lu Z, Wu J, Lin X, Jiang D, Cai Y, et al. Computational optical sectioning with an incoherent multiscale scattering model for light-field microscopy. *Nat Commun* 2021;12:6391.
- Wang Z, Zhu L, Zhang H, Li G, Yi C, Li Y, et al. Real-time volumetric reconstruction of biological dynamics with light-field microscopy and deep learning. *Nat Methods* 2021;18:551–6.
- Prevedel R, Yoon YG, Hoffmann M, Pak N, Wetzstein G, Kato S, et al. Simultaneous whole-animal 3d imaging of neuronal activity using light-field microscopy. *Nat Methods* 2014;11:727–30.
- Wagner N, Norlin N, Gierten J, De Medeiros G, Balázs B, Wittbrodt J, et al. Instantaneous isotropic volumetric imaging of fast biological processes. *Nat Methods* 2019;16:497–500.
- Yoon YG, Wang Z, Pak N, Park D, Dai P, Kang JS, et al. Sparse decomposition light-field microscopy for high speed imaging of neuronal activity. *Optica* 2020;7:1457–68.
- Galdón L, Saavedra G, Garcia-Sucerquia J, Martínez-Corral M, Sánchez-Ortiga E. Fourier lightfield microscopy: a practical design guide. *Appl Opt* 2022;61:2558–64.
- Grilli S, Paturzo M, Miccio L, Ferraro P. In situ investigation of periodic poling in congruent linbo3 by quantitative interference microscopy. *Meas Sci Technol* 2008;19:074008.
- Wang Z, Miccio L, Coppola S, Bianco V, Memmolo P, Tkachenko V, et al. Digital holography as metrology tool at micro-nanoscale for soft matter. *Light Adv Manuf* 2022;3:151–76.
- Mandracchia B, Wang Z, Ferraro V, Villone MM, Di Maio E, Maffettone PL, et al. Quantitative imaging of the complexity in liquid bubbles' evolution reveals the dynamics of film retraction. *Light: Sci Appl* 2019;8:20.
- Pritt MD, Shipman JS. Least-squares two-dimensional phase unwrapping using fft's. *IEEE Trans Geosci Remote Sens* 1994;32:706–8.